

Unexpected Metal–Insulator Transition in $\text{Ca}_{1-x}\text{Sr}_x\text{VO}_3$ Thick Film with Anomalous V Valence State

$\text{Ca}_{1-x}\text{Sr}_x\text{VO}_3$ thick films were fabricated on (100)-oriented SrTiO_3 substrates. In contradistinction to previous reports in which only extremely thin film (several nm thick) exhibited metal–insulator transition (MIT), MIT was observed for films with a thickness of 50 nm. To investigate the origin of the MIT, the electronic structure was examined using X-ray photoemission spectroscopy. An anomalous V valence state was observed in $V 2p_{3/2}$ spectra, which comprised four components (V^{5+} , V^{4+} , V^{3+} , and $V^{2+/1+}$). This chemical disorder may be caused by strain from the substrate. The observed MIT can be explained by an increment in electron–electron interactions due to this chemical disorder.

SrVO_3 and the derivative Ca-doped SrVO_3 ($\text{Ca}_{1-x}\text{Sr}_x\text{VO}_3$), which is a $3d^1$ perovskite, are typical bandwidth-controlled metal–insulator transition (MIT) materials, which are attracting attention for application to next-generation nanoelectronics due to their MIT [1–3]. However, MIT has only been achieved for ultrathin films (several nm thick) [1], which are not well suited for practical applications. MIT in an $\text{SrTi}_{1-x}\text{V}_x\text{O}_3$ thick film (16 nm) was reported recently [4]. Possible reasons for the emergence of MIT in the thick film were conjectured to be electron–electron interactions and disorder-induced localization. Thus, MIT in $\text{Ca}_{1-x}\text{Sr}_x\text{VO}_3$ thick film is expected if electron–electron interactions and/or the localization effect can be tuned in some manner.

The normalized electrical resistivity of $\text{Ca}_{1-x}\text{Sr}_x\text{VO}_3$ thick films measured by a four-probe method is shown in Figs. 1(a) and 1(b). Over the entire range, the resistivity of the films with $x = 0, 0.1$, and 1 can be expressed by a Fermi liquid model, i.e., $\rho = \rho_0 + AT^2$, where ρ_0 is a residual resistivity and A is the temperature coefficient of resistivity quantifying the electron–electron interactions in the strongly correlated Fermi liquid model. In contrast, films with $x = 0.2$ and 0.5 demonstrated resis-

tivity upturns at transition temperatures (T_{MIT}) of 72 and 113 K, respectively (indicated by the arrow). As the temperature was lowered from T_{MIT} , resistivity of these thin films exhibited semiconducting behavior. In a previous report, MIT in an SVO ultrathin film was attributed to dimensional crossover from a three-dimensional metal to a two-dimensional insulator [1]. However, in this study, the effect of dimensional crossover is not appropriate because the film thickness was 50 nm (not an ultrathin film). To determine the reason for the appearance of MIT, the electronic structure of $\text{Ca}_{1-x}\text{Sr}_x\text{VO}_3$ thick films was investigated using hard and soft X-ray photoemission spectroscopy (HX-PES; SX-PES) [5].

All HX-PES and SX-PES measurements were conducted at room temperature. The photon energy was 5953.4 eV for the HX-PES and 1486.6 eV for the SX-PES measurements. The surface sensitive SX-PES spectra of the $V 2p_{3/2}$ core level for the $\text{Ca}_{1-x}\text{Sr}_x\text{VO}_3$ thick films are shown in Fig. 2(a). The spectra were analyzed by deconvolving them into three components, i.e., V^{5+} (517.3 eV), V^{4+} (516.3 eV), and V^{3+} (514.3 eV). The intensity ratio between V^{5+} and V^{3+} was approximately 1:1 in the whole composition, which is attributed to

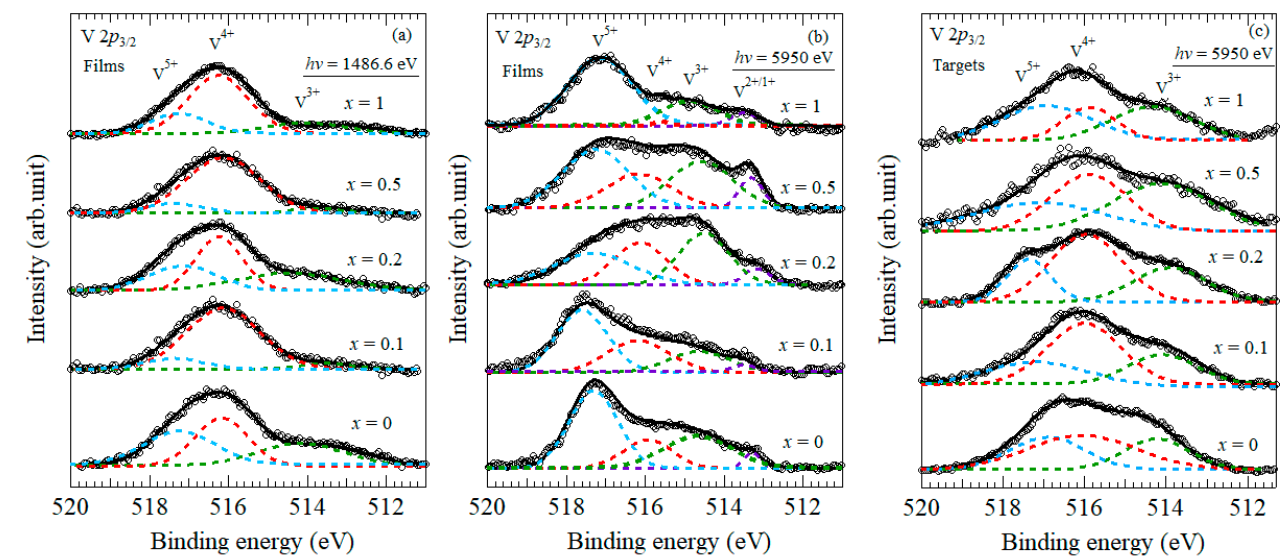


Figure 2: (a) SX-PES spectra of the $V 2p_{3/2}$ core level of $\text{Ca}_{1-x}\text{Sr}_x\text{VO}_3$ thick films. HX-PES spectra of the $V 2p_{3/2}$ of $\text{Ca}_{1-x}\text{Sr}_x\text{VO}_3$ (b) thick films and (c) targets are shown. Blue, red, green and purple lines indicate V^{5+} , V^{4+} , V^{3+} , and $V^{2+/1+}$ components, respectively. Black line indicates the sum of all contributing peaks (e.g., V^{5+} peaks).

phase separation of V^{4+} to V^{3+} and V^{5+} ($2V^{4+} \rightarrow V^{3+} + V^{5+}$) due to the strong correlation effects. These SX-PES results agree with the $\text{Ca}_{1-x}\text{Sr}_x\text{VO}_3$ bulk results obtained by Maiti *et al.* [6]. The bulk sensitive HX-PES results are shown in Fig. 2(b). The results differ drastically from those of SX-PES. The $V 2p_{3/2}$ spectra comprise four components, i.e., V^{5+} (517.4 eV), V^{4+} (516 eV), V^{3+} (514.6 eV), and $V^{2+/1+}$ (513.2 eV). The intensity of V^{5+} was the strongest, and this behavior cannot be explained by dismutation of V^{4+} due to the strong correlation. The $\text{Ca}_{1-x}\text{Sr}_x\text{VO}_3$ targets were also investigated by HX-PES, as shown in Fig. 2(c). The $V 2p_{3/2}$ spectra comprise V^{5+} , V^{4+} , and V^{3+} , which agree with the bulk results of Maiti *et al.* (including the intensity ratio between V^{5+} and V^{3+}) [6]. Thus, the extra component of $V^{2+/1+}$ is induced by being thinned. In this study, we focused on strain from the substrate due to lattice mismatch as a probable cause for that component. Generally, strain from the substrate reduces as film thickness increases, and the surface state then resembles the bulk free from strain. An inelastic mean free path calculated using the Tanuma-Powell-Penn equation [7, 8] is ~ 10 nm and ~ 3 nm for HX-PES and SX-PES measurements, respectively. Therefore, the HX-PES results reflect more bulk components with a relatively large strain effect, which can induce the anomalous V valence state. In strongly correlated systems, chemical disorder effects (e.g., $V^{2+/1+}/V^{3+}/V^{4+}/V^{5+}$) can drive MIT [9]. We have also confirmed that the electron localization effect was not a dominant reason for MIT based on the magnetoresistance behavior as a function of temperature [5]. Thus, we concluded that the dominant reason for MIT in the present case is likely an increment of electron–elec-

tron interactions resulting from the chemical disorder. In future studies, we will investigate how the thick film becomes distorted utilizing *in situ* observation methods including XRD, neutron diffraction, and Raman spectroscopy.

REFERENCES

- [1] K. Yoshimatsu, T. Okabe, H. Kumigashira, S. Okamoto, S. Aizaki, A. Fujimori and M. Oshima, *Phys. Rev. Lett.* **104**, 147601 (2010).
- [2] M. Takayanagi, T. Tsuchiya, W. Namiki, T. Higuchi and K. Terabe, *J. Phys. Soc. Jpn.* **87**, 034802 (2018).
- [3] M. Takayanagi, T. Tsuchiya, W. Namiki, Y. Kitagawa, D. Etoh, D. Nishioka, T. Yamada, T. Higuchi and K. Terabe, *Trans. Mater. Res. Soc. Jpn.* **44**, 57 (2019).
- [4] M. Gu, S. A. Wolf and J. Lu, *Appl. Phys. Lett.* **103**, 223110 (2013).
- [5] M. Takayanagi, T. Tsuchiya, W. Namiki, S. Ueda, M. Minohara, K. Horiba, H. Kumigashira, K. Terabe and T. Higuchi, *Appl. Phys. Lett.* **112**, 133106 (2018).
- [6] K. Maiti, D. D. Sarma, M. J. Rozenberg, I. H. Inoue, H. Makino, O. Goto, M. Pedio and R. Cimino, *Europhys. Lett.* **55**, 246 (2001).
- [7] S. Tanuma, C. J. Powell and D. R. Penn, *Surf. Interface Anal.* **11**, 577 (1988).
- [8] S. Tanuma, C. J. Powell and D. R. Penn, *Surf. Interface Anal.* **35**, 268 (2003).
- [9] M. Gu, J. Laverock, B. Chen, K. E. Smith, S. A. Wolf and J. Lu, *J. Appl. Phys.* **113**, 133704 (2013).

BEAMLIN

BL-2A

M. Takayanagi^{1,2}, T. Tsuchiya², W. Namiki^{1,2}, S. Ueda^{2,3}, M. Minohara⁴, K. Horiba⁴, H. Kumigashira⁴, K. Terabe² and T. Higuchi¹ (¹Tokyo Univ. of Sci., ²NIMS, ³Spring-8, ⁴KEK-IMSS-PF)

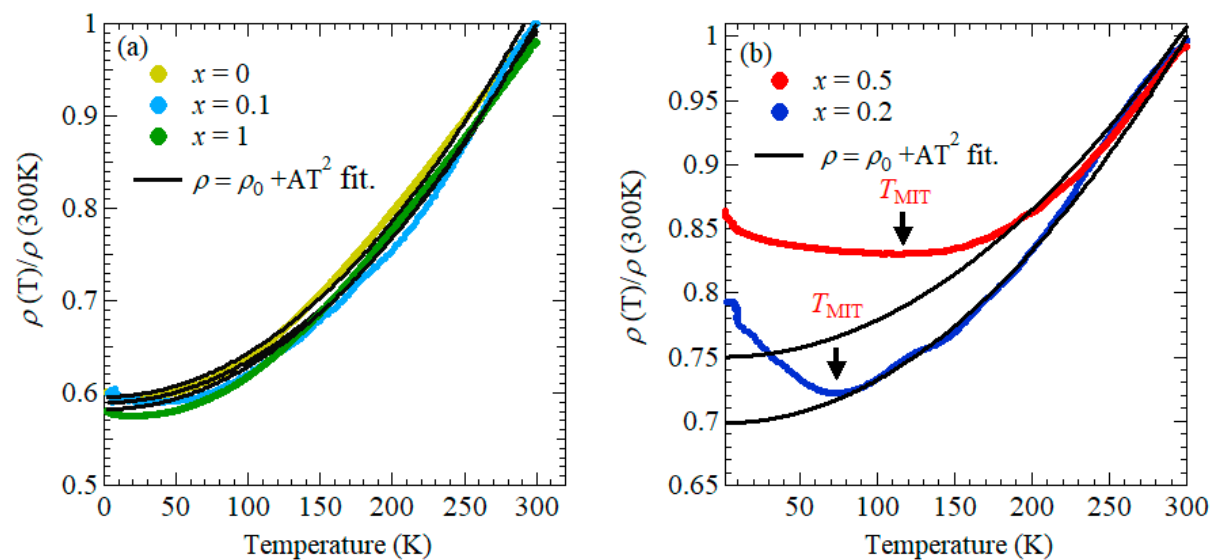


Figure 1: Temperature dependent normalized electrical resistivity for (a) $x = 1, 0.1$, and 0 and (b) $x = 0.5$ and 0.2. $\rho = \rho_0 + AT^2$ fits are also shown.